Published in final edited form as:
J Immunol. 2009 December 15; 183(12): 8004–8014. doi:10.4049/jimmunol.0901937.

In a murine tuberculosis model, the absence of homeostatic chemokines delay granuloma formation and protective immunity

Shabaana A. Khader[*,#,1], **Javier Rangel-Moreno**[*,†], **Jeffrey J. Fountain**[*], **Cynthia A Martino**[*], **William W Reiley**[*], **John E. Pearl**[*], **Gary M Winslow**[*,¶], **David L Woodland**[*], **Troy D Randall**[*,†], and **Andrea M. Cooper**[*]

[*] Trudeau Institute, Inc., Saranac Lake, NY 12983

[#] Children's Hospital of Pittsburgh, University of Pittsburgh School of Medicine, Pittsburgh PA 15213

[†] Department of Medicine, Division of Allergy, Immunology and Rheumatology, University of Rochester Medical Center, Rochester, NY 12642

[¶] Wadsworth Center, Albany, NY 12208

Abstract

Mycobacterium tuberculosis infection results in the generation of protective cellular immunity and formation of granulomatous structures in the lung. CXC chemokine ligand (CXCL)-13, CC chemokine ligand (CCL)-21 and CCL19 are constitutively expressed in the secondary lymphoid organs and play a dominant role in the homing of lymphocytes and dendritic cells. Although it is known that dendritic cell transport of *M. tuberculosis* from the lung to the draining lymph node is dependent on CCL19/CCL21, we show here that CCL19/CCL21 is also important for the accumulation of antigen-specific IFNγ-producing T cells in the lung, development of the granuloma, and control of mycobacteria. Importantly, we also show that CXCL13 is not required for generation of IFNγ responses, but is essential for the spatial arrangement of lymphocytes within granulomas, optimal activation of phagocytes and subsequent control of mycobacterial growth. Further, we show that these chemokines are also induced in the lung during the early immune responses following pulmonary *M. tuberculosis* infection. These results demonstrate that homeostatic chemokines perform distinct functions that cooperate to mediate effective expression of immunity against *M. tuberculosis* infection.

Introduction

Immunity to tuberculosis (TB) is characterized by the induction and recruitment of protective interferon gamma (IFNγ) producing T cells to the lungs, IFNγ-dependent activation of *Mycobacterium tuberculosis* (Mtb)-infected macrophages and subsequent mycobacterial control (1). The formation of an organized pulmonary granuloma containing recruited lymphocytes and mononuclear cells is essential for immunity and to limit tissue damage (2). However, the cascade of early signals that is induced following Mtb infection that mediate cell recruitment and granuloma formation are not well understood.

1Correspondence should be addressed to Shabaana A Khader, current address Children's Hospital of Pittsburgh, 530 45th Street, Pittsburgh PA 15201. Phone (412)-692-7767. Fax: (412)-692-7636. Shabaana.Khader@chp.edu.

2This work was supported by Career Development Award AI057158 (North East Biodefense Center-Lipkin), 1K99/R00AI075106-01, National Institute of Health, and Children's Hospital of Pittsburgh to SAK; HL69409 and AI072689 to TDR; AI073564 to DLW and GW, the Potts Foundation and the Trudeau Institute to DLW; AI 46530, AI-67723 and Trudeau Institute to AMC.

Homeostatic chemokines such as the CXC chemokine ligand 13 (CXCL13), CC chemokine ligand (CCL)19, and CCL21 are expressed in secondary lymphoid organs and direct the steady-state homing and localization of lymphocytes and dendritic cells within these organs (3,4). CCL19, CCL21 are expressed by stromal cells in the paracotical T cell zones and CCL21 is also expressed by high endothelial venules (HEVs) and the lymphatic endothelium (5–7). Both of these chemokines bind to their receptor CCR7 and direct the homing of naïve, central memory T cells and dendritic cells (DCs) to the secondary lymphoid organ (5–7). Recent evidence also suggests that the homeostatic chemokines CCL19/CCL21 provide signals that trigger DC transport of Mtb from the lung to the draining lymph node and are required for activation of T cells (8). Further, mice unable to express CCR7 fail to exhibit proper spatial organization of granulomas in response to Mtb infection (9). Although these data suggest an important role for CCL19/CCL21 in the generation of the acquired cellular response to Mtb, it is not known whether CCL19/CCL21 is important for the generation of antigen-specific IFNγ-producing T cells, accumulation of antigen-specific IFNγ-producing T cells, development of the granuloma, or for control of mycobacteria in the lung. CXCL13 is expressed by follicular DCs as well as by stromal cells in the B cell areas and orchestrates the homing of CXCR5 expressing lymphocytes to the follicular areas of the secondary lymphoid organs (10). It is not known whether the homeostatic chemokine CXCL13 is required for priming, initiation, or maintenance of immune responses to Mtb or whether it is essential for granuloma formation. Homeostatic chemokines are also induced in the lung during infection and inflammation and initiate the recruitment of immune cells (11,12). The accumulation of lymphocytes and mononuclear cells in response to infection and inflammation can resemble ectopic lymphoid follicles. These structures contain well established B and T cell areas, defined germinal centers and HEVs and have been termed ‘inducible bronchus associated lymphoid tissue’ (iBALT) (13). It has been suggested that granulomas resulting from Mtb infection contain areas that resemble ectopic lymphoid follicles both in humans (14) and mice (9,15). However, it is not known whether homeostatic chemokines have a role to play in the generation of lymphoid structures during TB.

To investigate the relationship between homeostatic chemokine expression and protective cellular responses and granuloma formation, we compared the immune response of wild type mice with those of mice lacking the homeostatic chemokines following Mtb infection. Normal mice posses at least two independent CCL21 genes, *Scya21a* and *Scya21b*. The *Scya21a* gene encodes a serine at position 65 of CCL21 (CCL21-Ser) and is known to be expressed in both secondary lymphoid organs and lymphatics. However, the *Scya21b* gene, encodes leucine at position 65 (CCL21-Leu) and is expressed only in the lymphatic endothelium of peripheral tissues. We have used *plt/plt* mice (16) which do not express CCL21-Ser (*Scya21a*) or CCL19 protein in secondary lymphoid organs but continue to express CCL21-Leu (*Scya21b*) at reduced levels in lymphatic endothelium (17,18). Further, the *plt/plt* mice demonstrate abnormalities in dendritic cell and lymphocyte migration as well as in lymph node organization and size (19,20). In the present study, using the *plt/plt* mice we show that CCL19/CCL21 is required for DC accumulation in the draining lymph nodes, optimal priming and generation of activated IFNγ-producing T cells, accumulation of IFNγ antigen-specific cells in the lung, granuloma formation and protection following Mtb challenge.

To determine the role of the homeostatic chemokine CXCL13 in response to Mtb infection, we used mice that lack the expression of CXCL13 (*Cxcl13*$^{-/-}$ mice) (21,22). *Cxcl13*$^{-/-}$ mice have defects in B cell trafficking (22,23), organization of B cells in the lymphoid organs (21), generation of germinal centers (24) and development of lymph nodes (21). Despite the lack of peripheral lymph nodes, we show that following Mtb challenge, *Cxcl13*$^{-/-}$ mice prime antigen-specific IFNγ-producing cells in the spleen, and accumulate activated T cells in the lungs similar to wild type mice. However, our data shows a novel role for CXCL13 in spatial organization of the lymphocytes within the inflammatory lesion, optimal activation of

phagocytes and control of Mtb. These data suggest that homeostatic chemokines CCL19/CCL21 and CXCL13 play distinct roles in initiation and maintenance of cellular responses that contribute to protective immunity and granuloma formation during Mtb infection.

Materials and Methods

Animals

C57BL/6 (B6) mice were purchased from The Jackson Laboratory (Bar Harbor, ME). *Cxcl13* −/− (22) and *plt/plt* mice (16) on the B6 background were obtained from J. Cyster (University of California, San Fransisco, CA) and bred at the Trudeau Institute. *plt/plt* mice were crossed with *Cxcl13*$^{-/-}$ mice to generate double knock out (DKO) mice. Early Secreted Antigenic Protein (ESAT6) αβTCR transgenic mice (Tg), recognize IA^{b}/ESAT6$_{1\text{-}20}$ and were generated by Drs. Gary Winslow (Wadsworth Center, Albany, NY) and David Woodland (Trudeau Institute, NY) (25). The ESAT6 TCR Tg mice were crossed to *Rag1*$^{-/-}$ mice. Experimental mice were age and sex matched and used between the ages of eight to ten weeks. Mice were used in accordance with National Research Council and Trudeau Institute IACUC guidelines.

Experimental infection

The H37Rv strain of Mtb was grown in Proskauer Beck medium containing 0.05% Tween 80 to mid-log phase and frozen in 1 ml aliquots at −70°C. For aerosol infections, animals were infected with ~75 bacteria using a Glas-Col (Terre Haute, IN) airborne infection system as described in detail (26).

Morphometric analysis and immunofluorescence

The lower right lobe of each lung was inflated with 10% neutral buffered formalin and processed routinely for light microscopy by hematoxylin and eosin stain (Colorado Histoprep, Fort Collins, CO). For immunofluorescence, paraffin was removed from the formalin-fixed lung sections, which were then washed with xylene, alcohol and PBS. Antigens were unmasked using a DakoCytomation Target Retrieval Solution and were blocked with 5%(v/v) normal donkey serum and Fc block (5 μg/ml: 2.4G27, Trudeau Institute Antibody Core Facility). Endogenous biotin was neutralized with avidin followed by biotin (Sigma Aldrich). Sections were probed with goat anti mouse CD3ε to detect CD3 lymphocytes (clone M-20; Santa Cruz Biotechnology), F4/80 to detect macrophages (Rat anti mouse F480, clone Cl: A3-1; Serotec), B220 to detect B cells (Rat anti mouse B220, clone RA3-6B2; BD Pharmingen) and iNOS to detect activated macrophages (Goat anti-iNOS, clone M-19; Santa Cruz Biotechnology). Primary antibodies were detected with secondary antibody conjugated to Cy-3 for iNOS and CD3 (Cy-3-Donkey Fab anti goat; Jackson Immunoresearch, West Grove, PA), donkey anti rat antibody conjugated to Alexa fluor 488 for F480 (Molecular probes, Eugene, OR) and SA-Alexa fluor 488 for B220 (Molecular probes, Eugene, OR). Slow fade gold antifade with DAPI (Molecular probes, Eugene, OR) was used to counterstain tissues and to detect nuclei. Images were obtained with a Zeiss Axioplan 2 microscope and were recorded with a Zeiss AxioCam digital camera. Caudal lobes from four mice per group underwent morphometric analysis in a blinded manner using the morphometric tool of Zeiss Axioplan microscope (Zeiss) which determines the area defined by the squared pixel value for each granuloma as described previously (27).

Lung and Draining Lymph Node (DLN) Cell preparation

Lung tissue and DLN was prepared as described (26). Briefly, a single cell suspension was prepared from either digested lung tissue or draining lymph node by dispersing the tissue through a 70μm nylon tissue strainer (BD Falcon, Bedford, MA). The resultant suspension was

treated with Gey's solution to remove any residual red blood cells, washed twice and counted (26).

Detection of IFN-γ producing cells by ELISpot assay

Antigen-specific IFN-γ-producing IA^b-restricted T cells from infected lungs or DLN were enumerated using peptide-driven ELISpot as previously described (28,29). Briefly, 96 well microtiter ELISpot plates were coated with monoclonal anti-mouse IFN-γ and then blocked with media containing 10% FBS. Cells from lungs and DLN were seeded at an initial concentration of 1×10^5 cells/well and subsequently diluted two fold. Irradiated B6 splenocytes were used as APC at a concentration of 1×10^6 cells/well in the presence of $ESAT\text{-}6_{1\text{-}20}$ (10 μg/ml) peptide and IL-2 (10U/ml) (28). After 24 h, plates were washed and probed with biotinylated anti-mouse IFN-γ. Spots were visualized and enumerated using a dissection microscope. No spots were detected in cultures lacking antigen or when using cells from uninfected mice.

Naive CD4 T cell isolation

To generate a population of Tg CD4 T cells from ESAT6 TCR Tg mice, a single cell suspension was prepared from lymph nodes and spleens by dispersing the tissues through a 70-μm nylon tissue strainer (BD Falcon). The single cell suspension was treated with Gey's solution to remove any residual red blood cells. Cells were subsequently panned on goat anti–mouse IgG H+L (Jackson ImmunoResearch Laboratories)-coated Primaria flasks (Falcon)for 45 min at 37°C, to remove B cells and macrophages. The Tg T cells were next enriched using a CD4 T cell negative isolation kit (Miltenyi Biotech, CA). A sample of the sorted cells was analyzed to confirm purity and to evaluate the surface expression of the activation markers CD69 and CD44. Purified Tg T cells were labeled with 0.5μm CFSE (Invitrogen/Molecular Probes, Eugene, OR) for 10 min at 37°C. 1×10^6 Tg T cells (200 μl) were transferred intravenously into Mtb infected mice. Twelve hours later, mice were sacrificed and the surface expression of CD69 and CD44 on transferred Tg T cells was determined.

Flow cytometry

Single cell suspensions were stained with fluorochrome-labeled antibodies specific for CD4 (clone GK1.5), CD69 (Clone HI2F3), CD44 (Clone IM7), CD11c (Clone HL3), MHC class II $I\text{-}A^b$ (Clone AF6-120.1), GL-7(Clone GL-7) and CD95 (Clone 15A7). Cells were collected on a Becton Dickinson FACSCalibur flow cytometer using CellQuest software or on a Dako CyAn™ ADP flow cytometer. Cells were gated based on their forward and side scatter characteristics and the frequency of specific cell types determined using FlowJo (Tree Star Inc, CA).

Real Time PCR

RNA was extracted from lung tissue as previously described(29). RNA samples were treated with DNAse and reverse transcribed. cDNA was then amplified using FAM-labeled probe and PCR primers on the ABI Prism 7700 sequence detection system. Fold increase in signal over that derived from uninfected lungs was determined using the ΔΔct calculation. The primer and probe sequence for murine *gapdh*, *Ifng*, *Tnf*, *inos* has been published (29). The oligonucleotides used for the detection of CCL21-Leu were designed and validated by the Trudeau Institute Molecular Biology Core Facility and were as follows: forward 5′-AGACTCAGGAGCCCAAAGCA-3′, reverse 5′GTTGAAGCAGGGCAAGGGT-3′, probe 5′FAM-CCACCTCATGCTGGCCTCCGT-BHQ. Primer and probes used for the detection of *Ccl19* and *Cxcl13* were purchased from Applied Biosystems.

Statistical Analysis

Differences between the means of experimental groups were analyzed using the two tailed Student's *t*-test. Differences were considered significant when $p \leq 0.05$.

Results

Homeostatic chemokines are induced in the lungs during the early immune response following Mtb infection

Mtb infection results in induction of homeostatic chemokines CCL19, CCL21 and CXCL13 in the lungs of infected mice (30). However, the kinetics of induction of these homeostatic chemokines in the lung during the early stages of infection are not known. To determine the timing of induction of homeostatic chemokines during the Mtb infection, we aerosol-infected wild type B6 mice with a low dose of Mtb and monitored the induction of mRNA for homeostatic chemokines in the lung. Sustained induction of mRNA for the homeostatic chemokines CCL19 and CXCL13 occurred between days 18 and 21 following infection (Fig 1A). Expression coincided with the induction of mRNA for IFNγ, TNFα, and iNOS in the lungs of infected mice (Fig 1B). In contrast, mRNA for CCL21 was not induced during infection. These data demonstrate that the homeostatic chemokines CCL19 and CXCL13, but not CCL21 are induced in the lung during the early phase of the immune response to Mtb infection and that this induction coincides with the expression of protective inflammatory responses in the lung.

A hallmark of immunity to Mtb is cellular accumulation and development of organized granulomatous response in the lung (2). To determine whether induction of chemokines correlated temporally with cellular events in the lung we followed the kinetics of initiation and generation of the granuloma formation in the lungs of Mtb-infected wild type B6 mice. The earliest signs of granuloma formation were evident by day 18 and progressed to the formation of well-established granulomata from day 21 through day 30 post infection (Fig 2A). Granuloma formation coincided with the recruitment of CD3 T cells and B220 cells on day 18 post infection (Fig 2B). The increase in size of the granulomata between days 21 and 30 (Fig 2A) coincided with the formation of distinct lymphoid-like structures in the lung. These included defined areas of B220 cells that were surrounded by CD3 lymphocytes (Fig 2B). Furthermore, the area occupied by the B220+ cells progressively increased from day 18 to day 30 post Mtb infection (Fig 2C,D). Thus, there is a temporal correlation between the induction of homeostatic chemokines, recruitment of lymphocytes and granuloma formation. The timing of these events also correlated with the expression of protective immune responses in the lung.

The expression of homeostatic chemokines is important for initiation of granuloma formation following Mtb infection

Following low dose aerosol infection with Mtb, the lungs of wild type mice developed a mononuclear infiltrate by day 20 post-infection (Fig 3 left panel) that progressed towards a mix of defined lymphocytic areas intermixed with macrophage aggregates by day 50 (Fig 3 middle panel). Well defined B220+ cell areas and activated iNOS producing macrophages were present by day 50 in wild type B6 mice (Fig 3 right panel). In contrast to the granulomatous response in wild type mice, the absence of either CCL19/CCL21 (*plt/plt* mice), CXCL13 (*Cxcl13*$^{-/-}$) or all homeostatic chemokines (DKO) resulted in poorly developed granulomata on day 20 (Fig 3 left panels). There was also a failure to develop the pronounced lymphocytic areas observed in the wild type on day 50 (figure 3 middle panels). Although iNOS-producing activated macrophages were detected in chemokine-deficient mice on day 50 post infection, the organization of defined B220+ cell areas in the lung was absent in the *Cxcl13*$^{-/-}$ and DKO infected lungs, and markedly compromised in the *plt/plt* mice (Fig 3 right panels). These data

suggested that in the absence of homeostatic chemokines, initiation and organization of lymphoid areas and granulomas in the lungs of infected mice is markedly disrupted.

Delayed accumulation of IFNγ producing T cells in the absence of CCL19/CCL21 but not CXCL13

Since the homeostatic chemokines are required for the development of the granulomatous response and organization of lymphoid areas in the lung, we next addressed whether there was a role for homeostatic chemokines in the acquired T cell response to infection. Analysis of intracellular IFNγ expression by CD4 lymphocytes from the lung demonstrated that the absence of CCL19/CCL21 (Fig 4A), but not CXCL13 (Fig 4B), ablated the accumulation of IFNγ producing cells in the infected lungs on day 20 post infection. When we determined the kinetics of the antigen-specific IFNγ response by ELISpot, we found that this response was delayed in the absence of CCL19/CCL21 but not in the absence of CXCL13 (Fig 4C). The delay in recruitment also correlated with a decreased frequency of activated CD44 high CD4 T cells in the lungs of *plt/plt* mice relative to B6 and *Cxcl13*$^{-/-}$ mice at day 20 post infection (data not shown). These data demonstrate that CCL19/CCL21, but not CXCL13 is required for early accumulation of antigen-specific IFNγ-producing cells in the lungs of Mtb-infected mice.

To investigate the impact of the homeostatic chemokine deficiency on the accumulation of activated antigen-specific cells within the infected lung, we adoptively transferred purified CFSE-labeled ESAT6 TCR Tg CD4 T cells into infected wild type and chemokine deficient mice at different time points post infection and compared the frequency of activated Tg cells accumulating in the lung. Twelve hours following transfer, the activation status of transferred ESAT6 TCR Tg T cells demonstrated that despite the absence of CXCL13, activated CD4 antigen-specific T cells accumulated in the lungs of day 20-infected mice (Fig 4D). In contrast, the absence of CCL19/CCL21 abrogated accumulation of activated CD4 antigen-specific T cells in the lungs of day 20 infected mice. These data suggest that CCL19/CCL21, but not CXCL13 are critical for accumulation of activated T cells during the early immune response in the lungs following Mtb infection.

To determine if the delayed accumulation of IFNγ producing cells in the infected lungs of *plt/plt* mice would impact expression of immunity, we evaluated the expression of protective molecules in the lung by real time PCR. mRNA transcripts for IFNγ and iNOS were induced in the lungs of infected B6 mice by day 20 and the transcript expression was maintained over time. However, the early induction of both IFNγ and iNOS mRNA was delayed in the *a*bsence of CCL19/CCL21 (Fig 5A). This delay also correlated with the absence of activated iNOS-producing F4/80-expressing macrophages in the *plt/plt* mice at day 20 compared to the B6 controls (Fig 5B). This deficiency was overcome by day 50 at both mRNA and protein levels for *iNOS* (Fig 5A,B). These data suggest that the delay in recruitment of activated IFNγ producing T cells to the lungs of *plt/plt* mice results in a delay in macrophage activation. To determine whether this delay in generation of acquired cellular responses affects bacterial control, B6 and *plt/plt mice* were infected with Mtb and the bacterial burden in the lungs determined (Fig 5C). The wild type B6 and *plt/plt* mice had similar bacterial burden in the lung on day 20 suggesting that initial infection and replication of the bacteria in the lungs of these mice were comparable. However, *plt/plt* mice were less able to limit bacterial growth after day 20 compared to the wild-type mice indicating that the delay in the generation of acquired immunity resulted in the establishment of higher bacterial numbers.

The generation of IFNγ producing T cells is compromised in the absence of CCL19/CCL21

The *plt/plt* mice have defective lymph nodes and compromised dendritic cell migration (7). Further, transport of Mtb to the lung draining lymph nodes via dendritic cells is likely to be dependent on CCL19/CCL21 (8), suggesting that poor accumulation of IFNγ-producing cells

in the infected lung could reflect poor induction of antigen-specific, IFNγ-producing T cell responses in lymph nodes. To address this issue, we compared the frequency and number of cells within the draining lymph nodes of wild type and *plt/plt* mutant mice. As expected, although numbers of white blood cells (WBCs) in the lungs of B6 and *plt/plt* mice were similar on day 20 following infection, the numbers of WBCs in draining lymph nodes of *plt/plt* mice were significantly lower (Fig 6A). Also as previously reported (8), the lymph nodes of *plt/plt* Mtb infected mice had markedly reduced frequencies and numbers of $CD11c^+$ cells (Fig 6B,C). In order to assess the impact of the reduced numbers of $CD11c^+$ cells on initiation of IFNγ T cell responses in the draining lymph nodes, we next evaluated the frequency of antigen-specific IFNγ-producing cells in the draining lymph nodes using ELISpot. Despite the low number of WBCs in the draining lymph nodes, and the decreased $CD11c^+$ cells in the lymph nodes, the frequency of antigen-specific IFNγ-producing cells in the infected *plt/plt* mice was similar to that detected in infected wild type mice (Fig 6D). However, despite this similar frequency, the reduced number of cells found in the *plt/plt* lymph nodes resulted in significantly fewer IFNγ-producing cells in the lymph nodes of infected *plt/plt* mice (Fig 6E). These data suggest that reduced DC accumulation in the draining lymph nodes in the *plt/plt* mice, results in induction of reduced magnitude of IFNγ responses in the lymphoid organs and delayed accumulation of IFNγ producing population in the lungs. Further, we also found reduced numbers of antigen-specific IFNγ producing cells in the spleens of day 20 infected *plt/plt* mice when compared to B6 infected mice (Fig 6F).

To further address the role of CCL19/CCL21 in initiation of Mtb-specific T cell responses, we analyzed the response of adoptively transferred CFSE-labeled ESAT-6 TCR Tg cells. On day 20 post infection, ESAT6 TCR Tg CD4T cells were transferred in to wild type and *plt/plt* mice and 12 hours later, the surface expression of CD69 on transferred cells within the draining lymph nodes was compared. We found that the frequency of Tg cells expressing CD69 in the lymph nodes of B6 and *plt/plt* mice was comparable (Fig 6G). These data suggest that despite the fact that *plt/plt* mice have several known defects in homing of T cells and DCs to the secondary lymphoid organs(7), activation and polarization of IFNγ T cells can occur in the absence of CCL19/CCL21. However the total number of cells in the lymph nodes of *plt/plt* mice were much lower and this likely impacts the kinetics of the accumulation of IFNγ producing cells in the lungs of *plt/plt* mice.

CXCL13 is required for spatial organization of lymphocytes within the granulomas

We expected that the comparable frequency and number of antigen-specific IFNγ producing cells in the lungs of wild type and *Cxcl13*$^{-/-}$ mice (Fig 4 B,C) would result in comparable induction of acquired immune responses following infection. To determine whether this was the case, we performed real time PCR analysis of infected lung tissue from wild type and *Cxcl13*$^{-/-}$ mice and found that the early expression of IFNγ, iNOS (Fig 7A) and TNFα (data not shown) were delayed in the lungs of *Cxcl13*$^{-/-}$ infected mice. To investigate this further, we compared the activation of $CD11b^+$ and $CD11c^+$ myeloid cells within the lungs of infected wild type and *Cxcl13*$^{-/-}$ mice. Despite the presence of equivalent numbers of activated T cells (data not shown) and IFNγ-producing T cells (Fig 4B,C), the induction of MHC Class II expression on CD11b and CD11c cells on day 20 post infection was significantly lower in infected *Cxcl13*$^{-/-}$ lungs, when compared to wild type mice (Fig 7B). This deficiency of expression of MHC Class II on CD11c cells in *Cxcl13*$^{-/-}$ mice was overcome by day 50 post infection. However, even at day 50 post infection, CD11b in lungs of infected *Cxcl13*$^{-/-}$ mice expressed significantly lower levels of MHC Class II expression when compared to B6 mice. Further, mRNA for 'Found in inflammatory zone' (FIZZ 1), a marker for alternatively activated macrophages (31, 32), was induced in the lungs of both B6 and *Cxcl13*$^{-/-}$ mice at day 20 post infection. The levels of Fizz1 mRNA transcripts were found to decrease between days 30 and 50 post infection in the B6 infected lungs. However, although the levels of Fizz1 mRNA

transcripts decreased in the lungs of *Cxcl13*$^{-/-}$ mice, they were significantly higher compared to B6 infected lungs at day 50 post infection (Fig 7C). The higher levels of Fizz1 mRNA found in the lungs of *Cxcl13*$^{-/-}$ lungs at day 50 post infection, suggests that macrophage activation may be skewed towards the alternative phenotype in the absence of CXCL13.

These data suggest that although IFNγ-producing T cells are recruited to the lungs of *Cxcl13*$^{-/-}$ infected mice, they are unable to effectively activate myeloid cells in the lung and to upregulate the expression of protective molecules during the early immune response. One possible explanation for the lack of CD11b and CD11c cell activation in the presence of activated CD4 T cells is that although protective cells are recruited to the lung, they are not spatially oriented within the granulomas for optimal activation of myeloid cells. Using immunofluorescence, we therefore determined the spatial location of CD3 T cells in the early granulomas in wild type, *plt/plt*, *Cxcl13*$^{-/-}$ and DKOs. The CD3 lymphocytes were dispersed throughout the granulomata in the wild type and *plt/plt* mice (Fig 7D). However, in the absence of CXCL13, the CD3 T cells accumulated in the lungs as distinct perivascular cuffs and were not detected within granulomata (Fig 7D). The area occupied by the perivascular cuff was significantly higher in *Cxcl13*$^{-/-}$ and DKO mice compared to B6 and *plt/plt* mice (Fig 7E). These data demonstrate that although CXCL13 was not required for generation and accumulation of activated IFNγ-producing cells to the lung, the recruited T cells required signals from CXCL13 in order to migrate into the granuloma and activate myeloid cells efficiently.

It has recently been shown that Germinal Center (GC) B cells are found in the lymphoid areas of the lung during chronic pulmonary tuberculosis (15). Therefore we also addressed whether GC B cells accumulated in the lungs of infected mice during the early immune response and whether this was dependent on CXCL13 expression. GC B cells (as identified by expression of GL-7 and CD95 (FAS)) did accumulate in the lungs at day 20 post infection following Mtb infection in wild type B6 mice (Fig 8A). This accumulation of GC B cells in the lungs was dependent on CXCL13 since the frequency of GC B cells was significantly reduced in the lungs of infected *Cxcl13*$^{-/-}$ mice. This suggests that CXCL13 plays a critical role in rapid accumulation of B and T cells during tuberculosis.

To determine whether the deficiency in cellular accumulation affected bacterial control, B6, *Cxcl13*$^{-/-}$ and DKO mice were infected with Mtb and the bacterial burden in the lungs determined (Fig 8B). B6, *Cxcl13*$^{-/-}$ and DKO mice all had similar levels of mycobacteria in the lung at day 20. However, unlike the wild-type mice, which controlled bacterial growth after day 20, neither the *Cxcl13*$^{-/-}$ nor the DKO mice were able to exhibit the same early control and had higher bacterial numbers in the lungs at subsequent time points. Further, the DKO mice were more susceptible than the *Cxcl13*$^{-/-}$ mice suggesting that the homeostatic chemokines CCL19/CCL21 and CXCL13 cooperate to initiate, generate and maintain protective immune responses during Mtb infection.

Discussion

The role of homeostatic chemokines in generation of the granuloma and in control of Mtb has not been definitively addressed. Our data show that homeostatic chemokines CCL19 and CXCL13 are induced in the lung during the early immune response following infection with Mtb. The induction of these homeostatic chemokines coincides with the induction of other protective molecules such as IFNγ, iNOS and TNFα as well as initiation of the granulomatous response and control of mycobacteria in the lungs of infected mice. Our data conclusively shows that the organization of the lymphoid structures and induction of protective immune responses during Mtb infection is dependent on homeostatic chemokine expression. Importantly, we show critical and yet distinct roles for individual homeostatic chemokines in

priming, recruitment and spatial arrangement of lymphocytes within the lymphoid areas during tuberculosis. Specifically, CCL19/21 are required for optimal priming, activation and accumulation of T cells in the lung, likely through their role in DC migration and priming of antigen-specific T cells responses in lymphoid organs. In contrast, we show that CXCL13 is not required for priming IFNγ-producing antigen-specific cells, but is critical for the spatial orientation of these cells within the granuloma in order to activate myeloid cells and control bacteria.

The delayed accumulation of IFNγ-producing cells in the lungs of *plt/plt* mice is likely caused by poor expansion of effector T cells in the lymph node rather than the failure of initiate T cell priming. For example, we find similar frequencies of antigen-specific IFNγ-producing cells in the lymph nodes of Mtb infected B6 and *plt/plt* mice. We also show that similar frequencies of adoptively transferred, naive ESAT-6-specific T cells become activated in the draining lymph nodes of Mtb-infected B6 and *plt/plt* mice, again suggesting that initial steps of T cell priming are intact. However, the lymph nodes of *plt/plt* mice are very small (19,20), so the total numbers of T cells that expand in the lymph nodes are limited. Previously published adoptive transfer experiments show that the activation and proliferation of Mtb Antigen 85-specific CD4 T cells in the lymph nodes is delayed in *plt/plt* mice following Mtb infection (33), but these authors did not look at whether this delay impacted accumulation of effector cells in the lungs. These authors also show that dendritic cell migration and the transport of Mtb to the draining lymph node is reduced in *plt/plt* mice (8) and suggest that this reduction is the limiting step in T cell priming (33). We also find reduced numbers of dendritic cells recruited to the draining lymph nodes of *plt/plt* mice. However, in both models, at least some level of T cell activation takes place in the lymph nodes of *plt/plt* mice (33).

We also find that T cells are effectively primed in *Cxcl13*$^{-/-}$ mice, which completely lack draining lymph nodes, but prime T cells effectively in the spleen. Thus, failure to expand in the lymph nodes cannot be the only explanation for reduced accumulation of IFNγ-producing T cells in the lungs of *plt/plt*-infected mice. In fact, other studies have demonstrated that homeostatic chemokines, such as CCL21, are important for attracting effector T cells to peripheral organs like the lung s(11). Moreover, we have found that CCL21ser and CCL19 are important for T cell responses to influenza in the lungs, independently of all secondary lymphoid organs (12). Thus, we conclude that, while disrupted lymph node architecture and poor dendritic cell accumulation in the lymph nodes of *plt/plt* mice likely contribute to poor T cell expansion and reduced early accumulation of IFNγ-producing T cells in the lungs, there are additional problems with effector cell recruitment to the lungs that also contribute to the reduced pulmonary IFNγ T cell responses.

Consistent with this idea, even when the T cell response eventually catches up in the *plt/plt* mice, the granulomatous response is severely compromised and nascent lymphoid areas fail to develop in *plt/plt* mice as they do in wild type infected lungs. CCL19 but not CCL21 is induced locally in the lung in response to Mtb infection and we propose that CCL19 is one of the primary homeostatic chemokines that is required for the initiation of the granulomatous response following Mtb infection. However we cannot formally rule out a role for CCL21 in granuloma formation. Although the T cell responses by day 30 are comparable between the *plt/plt* and the wild type mice, the increased bacterial growth in the *plt/plt* mice suggest that the failure to initiate granuloma formation limits the efficacy of the protective responses.

In contrast, absence of CXCL13 does not impact initial priming, activation and accumulation of activated IFNγ-producing T cells but compromises the ability of these cells to orient correctly within the granuloma and activate myeloid cells. Thus equivalent numbers of activated T cell numbers are generated and accumulate in the lungs of infected *Cxcl13*$^{-/-}$ mice but fail to interact with infected myeloid cells for bacterial control. The equivalent accumulation of

antigen-specific IFNγ-producing cells is in itself interesting in this model as T cell priming occurs despite the fact that *Cxcl13*$^{-/-}$ mice lack mediastinal draining lymph nodes. This means that the activation of T cells occurs elsewhere and indeed we have found equivalent numbers of IFNγ-producing cells in the spleens of day 20 infected *Cxcl13*$^{-/-}$ and wild type B6 mice. Further using the adoptive transfer model, we detected significantly higher frequency of newly activated ESAT-6 TCR Tg T cells (CD69 high) 12 hours following transfer in the spleens of day 20-infected *Cxcl13*$^{-/-}$ mice compared to the wild-type, suggesting that compensatory T cell activation was occurring in this organ. The basis for this enhanced splenic activation may relate to altered lymphatics and is not addressed in this text.

CXCL13 is known to recruit CXCR5-expressing lymphocytes into the lymphoid organs (23) and expression of CXCL13 has been strongly associated with the generation of ectopic lymphoid follicles (34,35). Our results demonstrate that CXCL13 is induced in the lung following Mtb infection and we propose that similar to the events occurring in the secondary lymphoid organs, activated lymphocytes that accumulate in the lung upregulate the expression of CXCR5 and respond to the CXCL13 produced in the inflamed Mtb infected lungs. This ligand receptor interaction then allows the T and B lymphocytes to orient themselves spatially within the lymphoid follicles. This event also appears critical for localization of T lymphocytes and macrophages within the granuloma for effective macrophage activation and bacterial control. Despite the accumulation of comparable numbers of IFNγ-producing cells in the lungs of *Cxcl13*$^{-/-}$ mice and B6 mice, defects in migration of activated T cells to macrophage areas in the *Cxcl13*$^{-/-}$ mice likely result in suboptimal or dysregulated activation of macrophages and higher bacterial burden. However diffusion of IFNγ from activated T cells located in the perivascular space may contribute to the limited control of bacteria seen in the lungs of *Cxcl13*$^{-/-}$ mice.

Recent evidence suggests that B cells form lymphoid follicles and may contribute to local immune responses in the lungs during chronic Mtb infection (15). We show that GC B cells accumulate in the lung during the early immune response following Mtb infection. Further, this accumulation of GC B cells is dependent on CXCL13 expression and impacts lymphoid neogenesis during Mtb infection. In this low dose aerosol model it is likely that the defect in the spatial orientation of T lymphocytes rather than a defect in the accumulation of GC B cells within lymphoid areas of Mtb infected *Cxcl13*−/− mice is responsible for the increased susceptibility. In support of this, B cell deficient mice clearly lack GCs, and yet they are not more susceptible than wild type B6 mice to low dose aerosol Mtb infection (15). These data for the first time show that induction of CXCL13 in the lung following Mtb infection is critical for recruitment of both B and T lymphocytes to the lung and for spatial orientation of lymphocytes within granulomas.

Our data also shows that DKO mice are more susceptible than *Cxcl13*$^{-/-}$ or *plt/plt* mice and have severe defects in lymphoid follicle organization, myeloid cell activation and recruitment of IFNγ producing cells to the lung. These data suggest that the homeostatic chemokines CXCL13 and CCL19/CCL21 cooperate to promote the generation of lymphoid follicles and induction of protective immune responses during Mtb infection.

Together our data define the sequential functions performed by homeostatic chemokines in the generation and expression of protective local immune responses against Mtb infection. Specifically, CCL19/CCL21 are required for optimal priming and generation of activated IFNγ producing T cells, while CXCL13 is critical for spatial organization of the lymphocytes within the inflammatory lesion. These homeostatic chemokines therefore play different roles but cooperate to generate an effective immune response for mycobacterial control.

References

1. Flynn J, Chan J. Immunology of tuberculosis. Annual Review of Immunology 2001;19:93–129.
2. Bean AG, Roach DR, Briscoe H, France MP, Korner H, Sedgwick JD, Britton WJ. Structural deficiencies in granuloma formation in TNF gene-targeted mice underlie the heightened susceptibility to aerosol Mycobacterium tuberculosis infection, which is not compensated for by lymphotoxin. J Immunol 1999;162:3504–3511. [PubMed: 10092807]
3. Cyster JG. Chemokines and cell migration in secondary lymphoid organs. Science 1999;286:2098–2102. [PubMed: 10617422]
4. Cyster JG. Chemokines and the homing of dendritic cells to the T cell areas of lymphoid organs. J Exp Med 1999;189:447–450. [PubMed: 9927506]
5. Gunn MD, Tangemann K, Tam C, Cyster JG, Rosen SD, Williams LT. A chemokine expressed in lymphoid high endothelial venules promotes the adhesion and chemotaxis of naive T lymphocytes. Proc Natl Acad Sci U S A 1998;95:258–263. [PubMed: 9419363]
6. Saeki H, Moore AM, Brown MJ, Hwang ST. Cutting edge: secondary lymphoid-tissue chemokine (SLC) and CC chemokine receptor 7 (CCR7) participate in the emigration pathway of mature dendritic cells from the skin to regional lymph nodes. J Immunol 1999;162:2472–2475. [PubMed: 10072485]
7. Gunn MD, Kyuwa S, Tam C, Kakiuchi T, Matsuzawa A, Williams LT, Nakano H. Mice lacking expression of secondary lymphoid organ chemokine have defects in lymphocyte homing and dendritic cell localization. J Exp Med 1999;189:451–460. [PubMed: 9927507]
8. Wolf AJ, Linas B, Trevejo-Nunez GJ, Kincaid E, Tamura T, Takatsu K, Ernst JD. Mycobacterium tuberculosis infects dendritic cells with high frequency and impairs their function in vivo. J Immunol 2007;179:2509–2519. [PubMed: 17675513]
9. Kahnert A, Hopken UE, Stein M, Bandermann S, Lipp M, Kaufmann SH. Mycobacterium tuberculosis triggers formation of lymphoid structure in murine lungs. J Infect Dis 2007;195:46–54. [PubMed: 17152008]
10. Legler DF, Loetscher M, Roos RS, Clark-Lewis I, Baggiolini M, Moser B. B cell-attracting chemokine 1, a human CXC chemokine expressed in lymphoid tissues, selectively attracts B lymphocytes via BLR1/CXCR5. J Exp Med 1998;187:655–660. [PubMed: 9463416]
11. Lo JC, Chin RK, Lee Y, Kang HS, Wang Y, Weinstock JV, Banks T, Ware CF, Franzoso G, Fu YX. Differential regulation of CCL21 in lymphoid/nonlymphoid tissues for effectively attracting T cells to peripheral tissues. J Clin Invest 2003;112:1495–1505. [PubMed: 14617751]
12. Rangel-Moreno J, Moyron-Quiroz JE, Hartson L, Kusser K, Randall TD. Pulmonary expression of CXC chemokine ligand 13, CC chemokine ligand 19, and CC chemokine ligand 21 is essential for local immunity to influenza. Proc Natl Acad Sci U S A 2007;104:10577–10582. [PubMed: 17563386]
13. Carragher DM, Rangel-Moreno J, Randall TD. Ectopic lymphoid tissues and local immunity. Semin Immunol 2008;20:26–42. [PubMed: 18243731]
14. Tsai MC, Chakravarty S, Zhu G, Xu J, Tanaka K, Koch C, Tufariello J, Flynn J, Chan J. Characterization of the tuberculous granuloma in murine and human lungs: cellular composition and relative tissue oxygen tension. Cell Microbiol 2006;8:218–232. [PubMed: 16441433]
15. Maglione PJ, Xu J, Chan J. B cells moderate inflammatory progression and enhance bacterial containment upon pulmonary challenge with Mycobacterium tuberculosis. J Immunol 2007;178:7222–7234. [PubMed: 17513771]
16. Nakano H, Mori S, Yonekawa H, Nariuchi H, Matsuzawa A, Kakiuchi T. A novel mutant gene involved in T-lymphocyte-specific homing into peripheral lymphoid organs on mouse chromosome 4. Blood 1998;91:2886–2895. [PubMed: 9531599]
17. Luther SA, Tang HL, Hyman PL, Farr AG, Cyster JG. Coexpression of the chemokines ELC and SLC by T zone stromal cells and deletion of the ELC gene in the plt/plt mouse. Proc Natl Acad Sci U S A 2000;97:12694–12699. [PubMed: 11070085]
18. Vassileva G, Soto H, Zlotnik A, Nakano H, Kakiuchi T, Hedrick JA, Lira SA. The reduced expression of 6Ckine in the plt mouse results from the deletion of one of two 6Ckine genes. J Exp Med 1999;190:1183–1188. [PubMed: 10523616]
19. Gunn MD. Chemokine mediated control of dendritic cell migration and function. Semin Immunol 2003;15:271–276. [PubMed: 15001176]

20. Nakano H, Gunn MD. Gene duplications at the chemokine locus on mouse chromosome 4: multiple strain-specific haplotypes and the deletion of secondary lymphoid-organ chemokine and EBI-1 ligand chemokine genes in the plt mutation. J Immunol 2001;166:361–369. [PubMed: 11123313]
21. Ansel KM V, Ngo N, Hyman PL, Luther SA, Forster R, Sedgwick JD, Browning JL, Lipp M, Cyster JG. A chemokine-driven positive feedback loop organizes lymphoid follicles. Nature 2000;406:309–314. [PubMed: 10917533]
22. Ansel KM, Harris RB, Cyster JG. CXCL13 is required for B1 cell homing, natural antibody production, and body cavity immunity. Immunity 2002;16:67–76. [PubMed: 11825566]
23. Ebisuno Y, Tanaka T, Kanemitsu N, Kanda H, Yamaguchi K, Kaisho T, Akira S, Miyasaka M. Cutting edge: the B cell chemokine CXC chemokine ligand 13/B lymphocyte chemoattractant is expressed in the high endothelial venules of lymph nodes and Peyer's patches and affects B cell trafficking across high endothelial venules. J Immunol 2003;171:1642–1646. [PubMed: 12902460]
24. Allen CD, Ansel KM, Low C, Lesley R, Tamamura H, Fujii N, Cyster JG. Germinal center dark and light zone organization is mediated by CXCR4 and CXCR5. Nat Immunol 2004;5:943–952. [PubMed: 15300245]
25. Reiley WW, Calayag MD, Wittmer ST, Huntington JL, Pearl JE, Fountain JJ, Martino CA, Roberts AD, Cooper AM, Winslow GM, Woodland DL. ESAT-6-specific CD4 T cell responses to aerosol Mycobacterium tuberculosis infection are initiated in the mediastinal lymph nodes. Proc Natl Acad Sci U S A 2008;105:10961–10966. [PubMed: 18667699]
26. Roberts, A.; Cooper, A.; Belisle, J.; Turner, J.; Gonzalez-Juarerro, M.; Orme, I. Murine Models of Tuberculosis. In: Kaufmann, S.; Kabelitz, D., editors. Methods in Microbiology. Academic Press; London: 2002. p. 433-462.
27. Khader SA, Bell GK, Pearl JE, Fountain JJ, Rangel-Moreno J, Cilley GE, Shen F, Eaton SM, Gaffen SL, Swain SL, Locksley RM, Haynes L, Randall TD, Cooper AM. IL-23 and IL-17 in the establishment of protective pulmonary CD4+ T cell responses after vaccination and during Mycobacterium tuberculosis challenge. Nat Immunol 2007;8:369–377. [PubMed: 17351619]
28. Winslow GM, Roberts AD, Blackman MA, Woodland DL. Persistence and turnover of antigen-specific CD4 T cells during chronic tuberculosis infection in the mouse. J Immunol 2003;170:2046–2052. [PubMed: 12574375]
29. Khader SA, Pearl JE, Sakamoto K, Gilmartin L, Bell GK, Jelley-Gibbs DM, Ghilardi N, deSauvage F, Cooper AM. IL-23 compensates for the absence of IL-12p70 and is essential for the IL-17 response during tuberculosis but is dispensable for protection and antigen-specific IFN-gamma responses if IL-12p70 is available. J Immunol 2005;175:788–795. [PubMed: 16002675]
30. Schreiber T, Ehlers S, Aly S, Holscher A, Hartmann S, Lipp M, Lowe JB, Holscher C. Selectin ligand-independent priming and maintenance of T cell immunity during airborne tuberculosis. J Immunol 2006;176:1131–1140. [PubMed: 16394002]
31. Raes G, De Baetselier P, Noel W, Beschin A, Brombacher F, Hassanzadeh Gh G. Differential expression of FIZZ1 and Ym1 in alternatively versus classically activated macrophages. J Leukoc Biol 2002;71:597–602. [PubMed: 11927645]
32. Raes G, Noel W, Beschin A, Brys L, de Baetselier P, Hassanzadeh GH. FIZZ1 and Ym as tools to discriminate between differentially activated macrophages. Dev Immunol 2002;9:151–159. [PubMed: 12892049]
33. Wolf AJ, Desvignes L, Linas B, Banaiee N, Tamura T, Takatsu K, Ernst JD. Initiation of the adaptive immune response to Mycobacterium tuberculosis depends on antigen production in the local lymph node, not the lungs. J Exp Med 2008;205:105–115. [PubMed: 18158321]
34. Luther SA, Lopez T, Bai W, Hanahan D, Cyster JG. BLC expression in pancreatic islets causes B cell recruitment and lymphotoxin-dependent lymphoid neogenesis. Immunity 2000;12:471–481. [PubMed: 10843380]
35. Rangel-Moreno J, Hartson L, Navarro C, Gaxiola M, Selman M, Randall T. Inducible bronchus-associated lymphoid tissue (iBALT) in patients with pulmonary complications of rheumatoid arthritis. Journal of Clinical Investigations 2006;116:3183–3194.

Abbreviations

TB	Tuberculosis
Mtb	Mycobacterium tuberculosis
CXCL	CXC chemokine ligand
CCL	CC chemokine ligand
IFNγ	Interferon gamma
HEVs	high endothelial venules

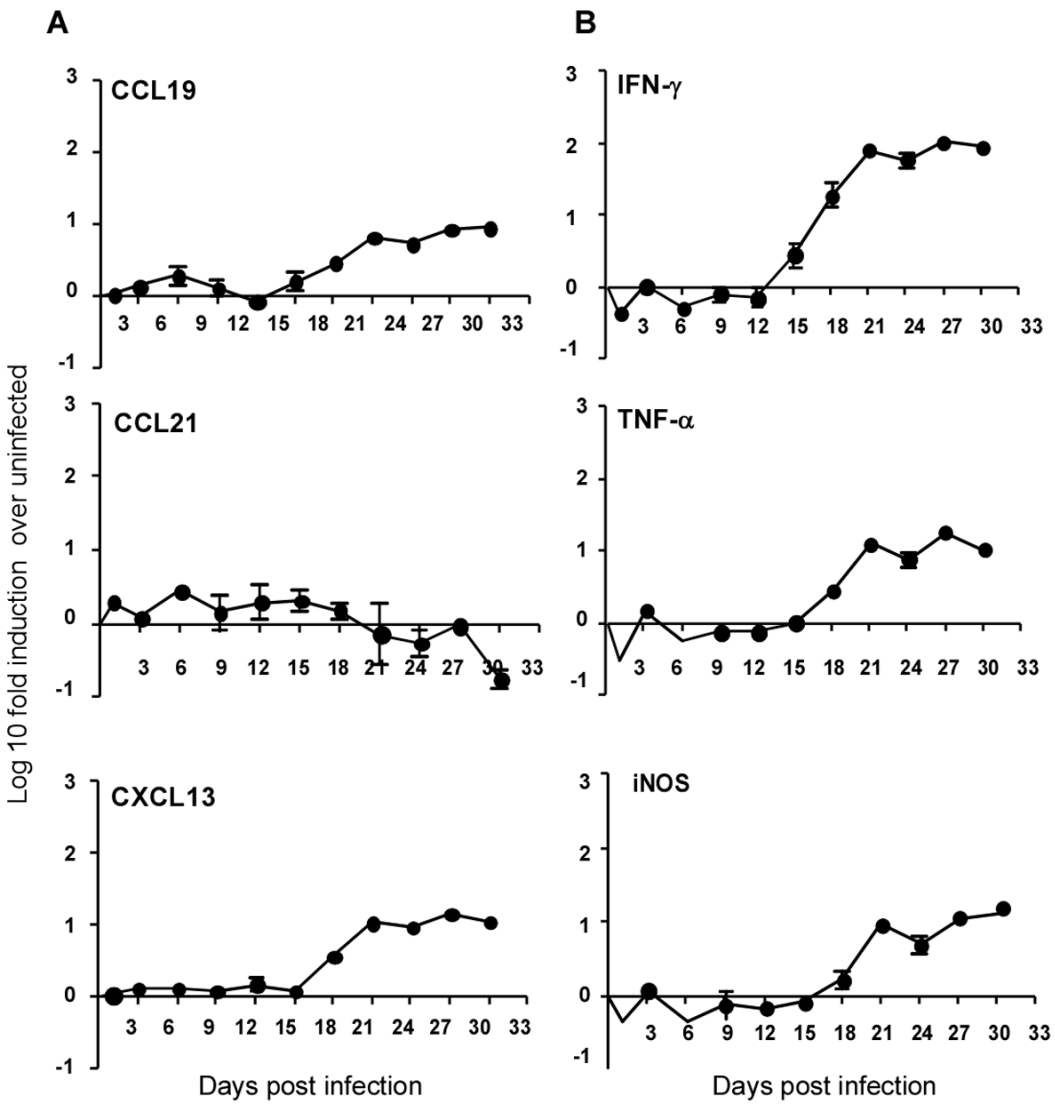

Figure 1. Homeostatic chemokines are induced in the lungs during the early immune response following Mtb infection

B6 mice were infected with ~75 CFU Mtb via the aerosol route and at specific times after infection, lung tissue was harvested and processed to extract RNA. The presence of mRNA for different homeostatic chemokines CCL19, CCL21 and CXCL13 (A) and protective molecules IFNγ, TNFα and iNOS (B) was determined by real-time PCR, and the $\log_{10}$ fold-increase in mRNA was determined for four infected mice vs four uninfected mice. The data points represent the mean and SD for four mice for each time point. One experiment representative of two shown.

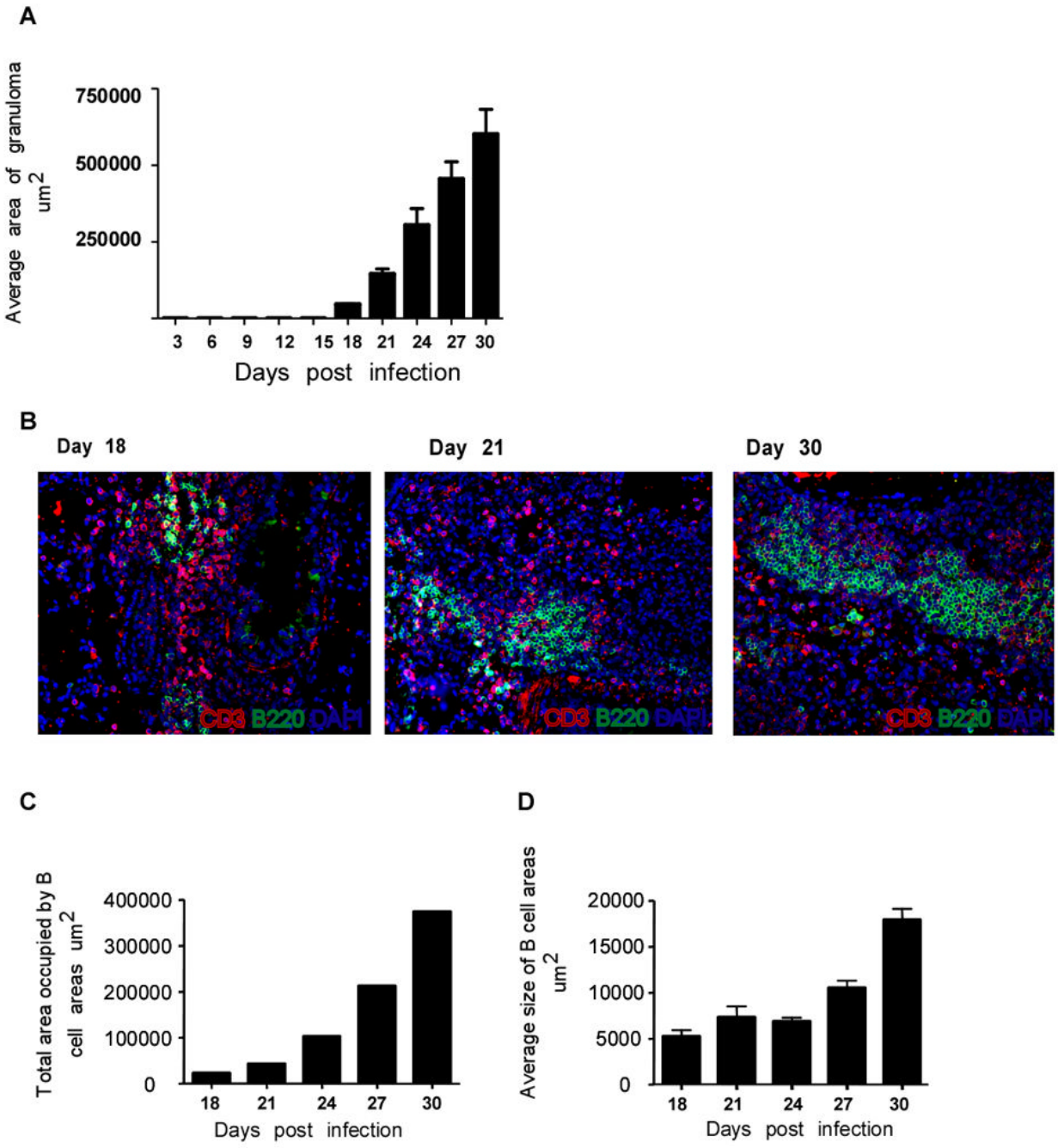

Figure 2. Early induction of homeostatic chemokines correlate with the initiation of granuloma formation in the lung following Mtb infection

B6 mice were infected as described in Figure 1. Upon harvest, the caudal lobe of the lung from each of four mice per group was perfused with 10% formal saline, embedded in paraffin, sectioned, and stained using H&E. Morphometric analysis of area covered by the granuloma in H & E stained sections of Mtb-infected B6 lungs at different time points during the early immune response was determined(A). The data points represent the mean and SD for four mice for each time point. Lung sections from infected B6 mice at different time points post infection were stained for B220 (green) and CD3 (red) and shown at 40x magnification (B). Representative of four mice per group. Morphometric analysis of total area (C) and average

area (D) covered by the B cell areas (B220+) in sections of infected lungs of B6 mice at different time points following infection. The data points represent the mean and SD for four mice for each time point. One experiment representative of two shown.

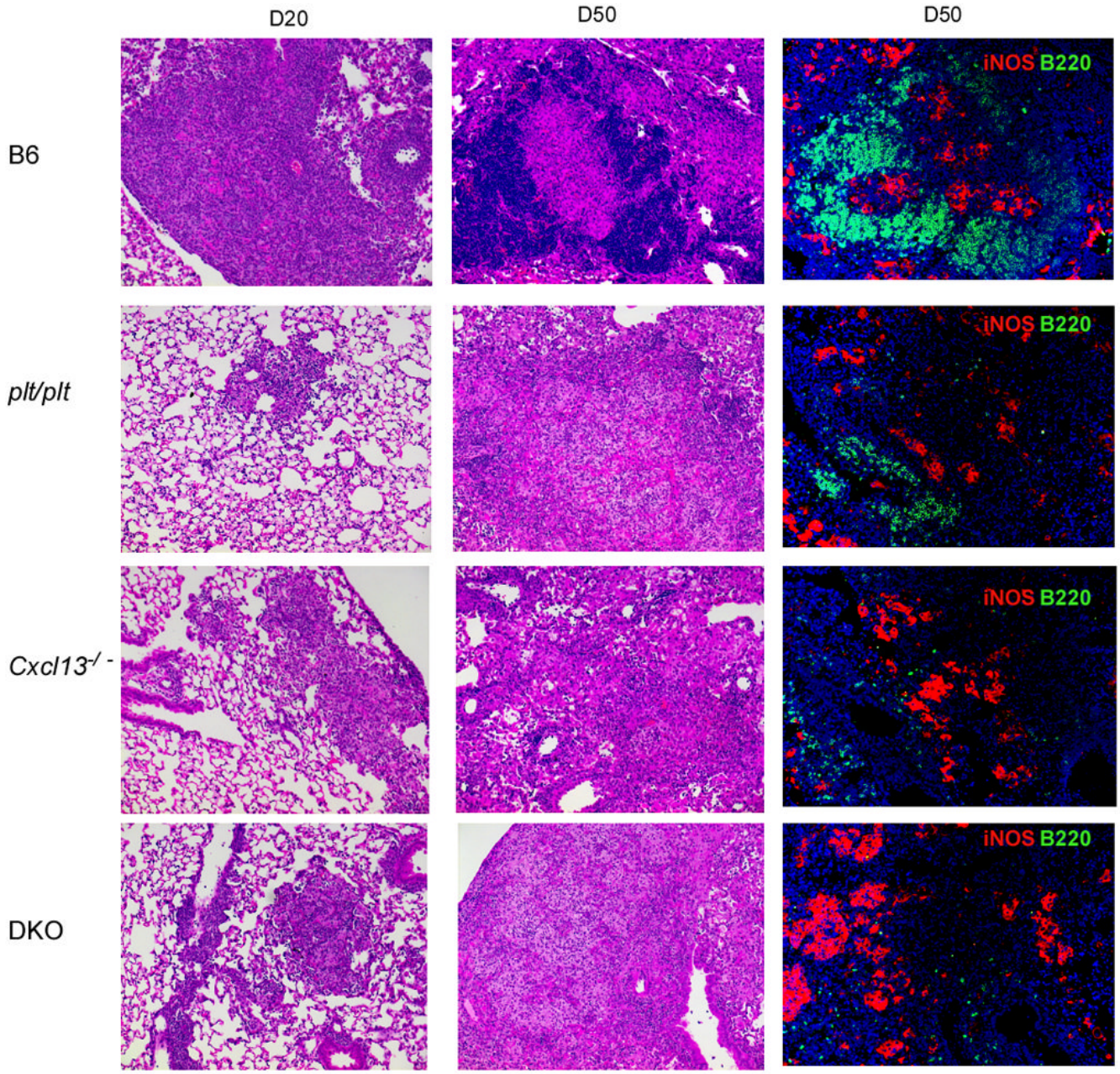

Figure 3. Expression of homeostatic chemokines is important for initiation and maintenance of granuloma formation following Mtb infection

B6 and chemokine deficient mice were infected as described for Figure 1 and lungs were fixed in 10% formalin, embedded in paraffin and stained using H &E as described in Figure 2. The panels in the left column show infected lungs (x10) at day 20 post infection. The panels in the middle column show the cellular components of the granulomata at day 50 post infection (x10). Areas of lymphocyte accumulation appear as darker areas, while areas of macrophage accumulation appear lighter. The panels in the right column show immunofluorescence for B cells (B220 in green) and iNOS (red) on day 50 post infection (x20). One experiment representative of two is shown, $n = 4$ mice per group.

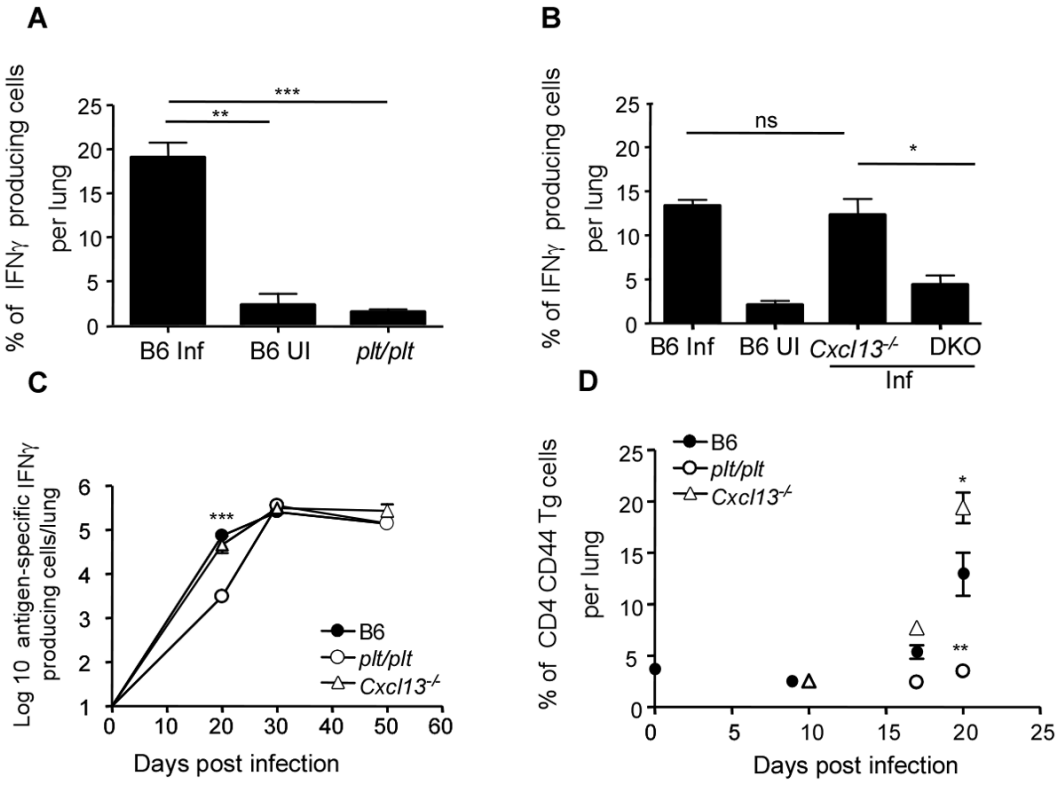

Figure 4. Delayed accumulation of IFNγ producing T cells in the absence of CCL19/CCL21 but not CXCL13

B6 (B6 Inf) and *plt/plt* mice (A) or B6 (B6 Inf), *Cxcl13*$^{-/-}$ and DKOs (B) were infected as in Figure 1. B6 uninfected controls are also shown (B6 UI)(A,B). Lymphocytes were isolated from the lung at day 20 post infection and were cultured with PMA/Ionomycin in the presence of golgi stop for 5 hours. The presence of intracellular IFNγ in CD4 T lymphocytes was determined by flow cytometry (A,B). Cells from infected B6 (closed circles), *plt/plt* (open circles), *Cxcl13*$^{-/-}$ (open triangles) were cultured with irradiated feeder cells and ESAT 6 peptide for 24 h and the number of IFN-γ producing antigen-specific cells determined by ELISpot(C). 1×10^6 ESAT-6 TCR Tg CSFE labeled naïve T cells were transferred into infected B6 (closed circles), *plt/plt* (open circles) or *Cxcl13*$^{-/-}$(open triangles) mice at different time points post infection (D). The expression of CD44 on transferred Tg T cells was determined 12 hours later. The data points represent the mean (±SD) of values from four-five mice (*A*, B, *C*, and *D*). * , $p \leq 0.05$. * * , $p \leq 0.005$. * * * , $p \leq 0.0005$. ns-not significant.

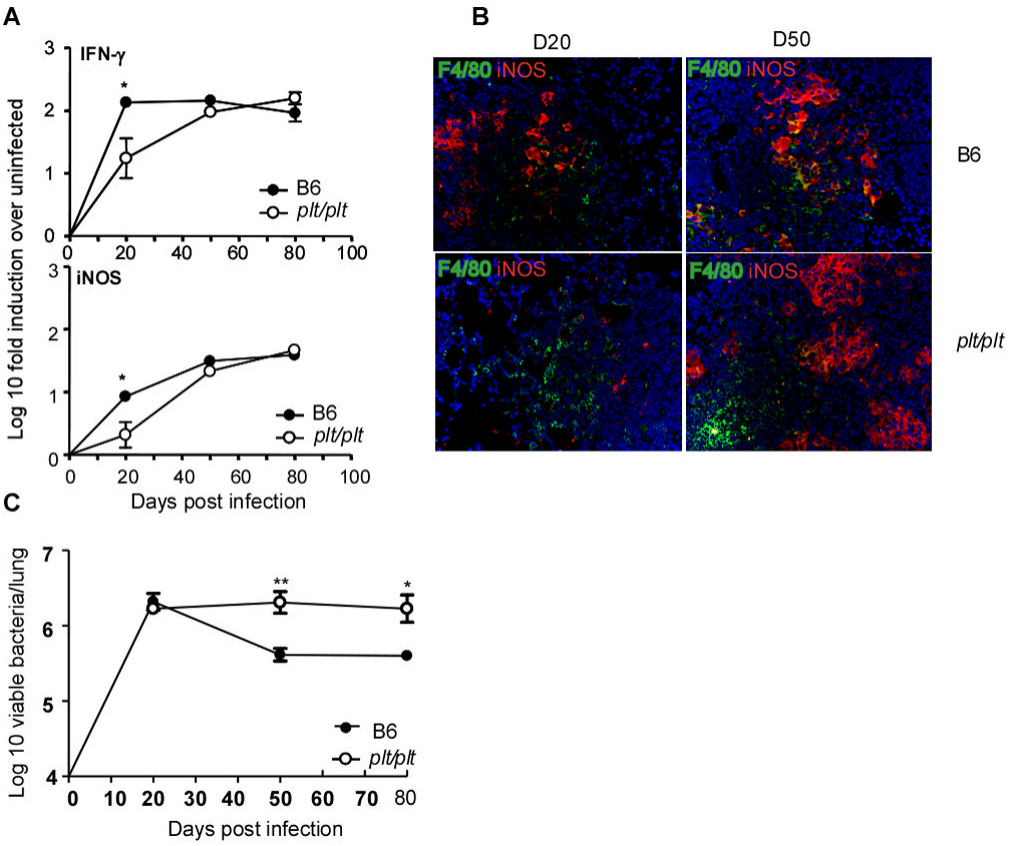

Figure 5. Delay in the generation of protective acquired responses in *plt/plt* mice results in establishment of higher bacterial numbers

B6 (closed circles) and *plt/plt* mice (open circles) were infected as described for Figure 1 and at various times post infection lung tissue was harvested and processed to extract RNA (A). The presence of specific mRNA was determined by real-time PCR and the $\log_{10}$-fold-increase determined for three to four infected mice over four uninfected mice. The data points represent the mean and SD values for four mice for each time point. The expression of iNOS (red) by macrophages expressing F4/80 (green) in lungs from Mtb infected B6 and *plt/plt* mice was determined at day 20 and day 50 post infection (B). B6 (closed circles) and *plt/plt* (open circles) mice were infected via the aerosol route with ~ 75 *M. tuberculosis* H37Rv bacteria. The bacterial burden was determined in the lungs of B6 and *plt/plt* infected mice over time(C). The graph shows one experiment representative of two. The data points represent the mean (±SD) of values from four-five mice (A, C). * , $p \leq 0.05$. * * , $p \leq 0.005$.

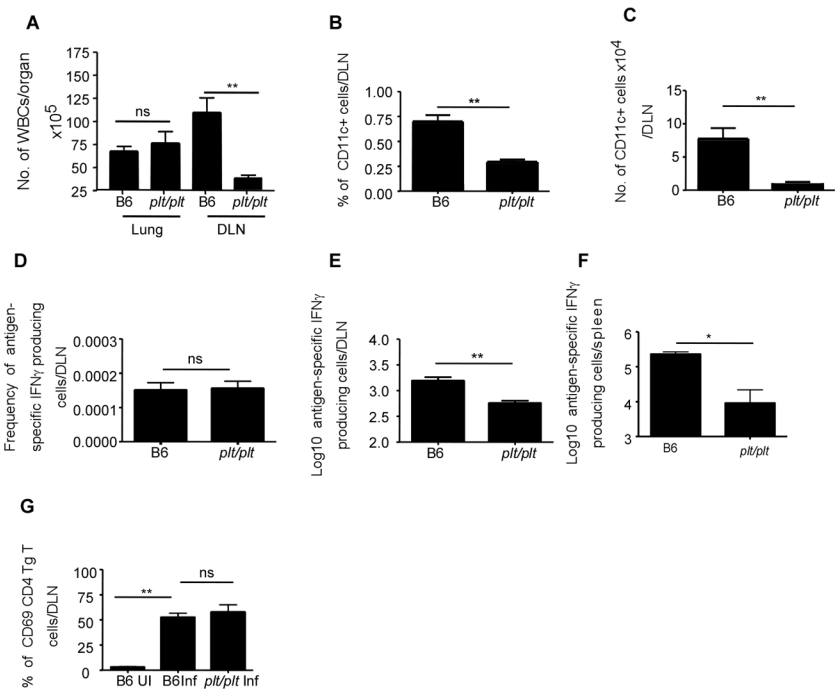

Figure 6. Compromised generation of IFNγ producing T cells in the absence of CCL19/CCL21

B6 and *plt/plt* mice were infected as described for Figure 1. Cells from wild type and *plt/plt* infected lungs and draining lymph nodes were isolated at day 20 and total numbers of WBCs were determined per organ (A). The frequency(B) of $CD11c^+$ cells in the lymph nodes of B6 and *plt/plt* mice were determined by flow cytometry and total numbers of $CD11c^+$ cells was determined(C). The frequency (D) and total numbers (E,F) of IFNγ producing antigen specific cells were determined by ESAT-6 driven ELISpot assay in draining lymph nodes (E) and spleen (F). 1×10^6 ESAT-6 TCR Tg CSFE labeled naïve T cells were transferred into infected B6 and *plt/plt* mice at day 20 post infection and the lymph nodes were harvested and processed to generate single cell suspensions 12 hours later(F). The expression of CD69 was determined on transferred Tg CD4 T cells using flow cytometry. The data points represent the mean (±SD) of values from four-five mice (A–F). * , $p \leq 0.05$. * * , $p \leq 0.005$, ns-not significant.

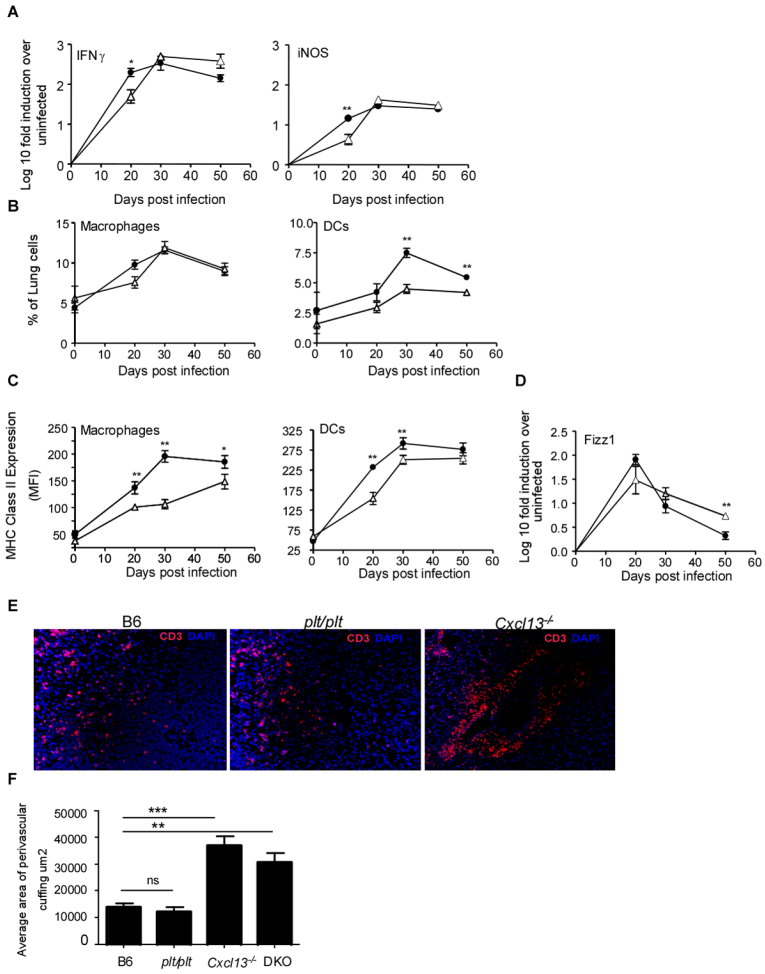

Figure 7. CXCL13 is required for spatial organization of lymphocytes within the granulomas

B6 (closed circles) and *Cxcl13*$^{-/-}$ mice (open triangles) were infected as described for Figure 1 and at specific times post infection lung tissue was harvested and processed to extract RNA (A). The presence of specific mRNA was determined by real-time PCR and the $\log_{10}$-fold-increase in mRNA determined for three to four infected mice vs four uninfected mice. The data points represent the mean and SD values for four mice for each time point. Expression of MHC Class II was determined on CD11b^{+} and CD11c^{+} cells isolated from lungs of infected B6 (filled circles) or *Cxcl13*$^{-/-}$ mice (open traingles) on day 20 post infection(B). The presence of Fizz 1 mRNA was determined by real-time PCR and the $\log_{10}$-fold-increase in mRNA determined for three to four infected mice vs four uninfected mice (C). The distribution of CD3 lymphocytes in lungs of infected B6, *plt/plt* and *Cxcl13*$^{-/-}$ mice was determined by immunofluorescence on day20 (D) and the area occupied by CD3 T lymphocytes in the perivascular cuffs was determined morphometrically (E).

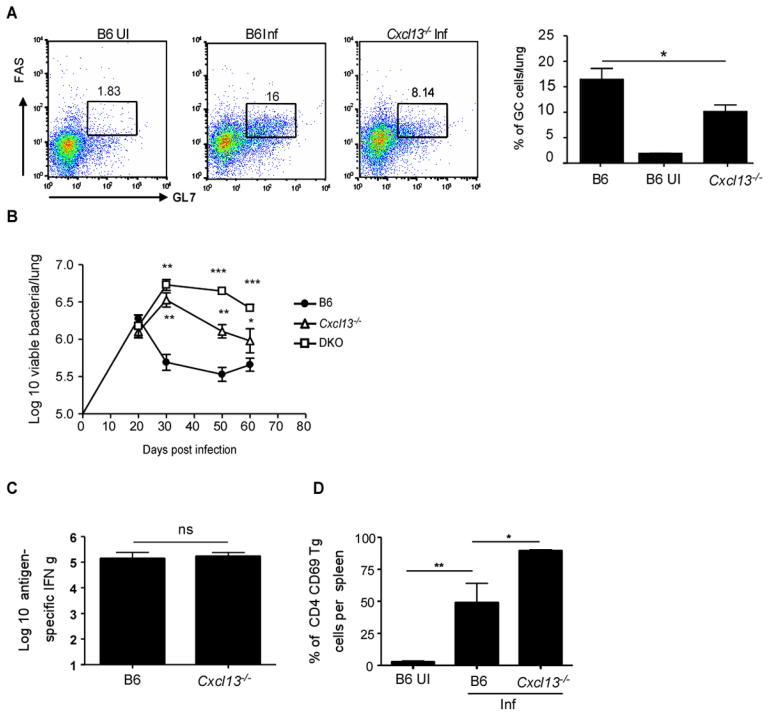

Figure 8. CXCL13 is required for recruitment of GC B cells and control of mycobacteria

B6 and *Cxcl13*$^{-/-}$ mice were infected as described for Figure 1 and the frequency of CD19/B220 positive B cells expressing GL7 and CD95/FAS (GC B cells) from lungs of infected B6 and *Cxcl13*$^{-/-}$ mice was determined by flow cytometry at day 20 post infection (A). B6 uninfected controls are also shown (B6 UI). B6 (closed circles), *Cxcl13*$^{-/-}$ (open triangles) and DKO (open squares) were infected via the aerosol route with 75 *M. tuberculosis* H37Rv bacteria and the bacterial burden determined in the lungs over time(B). B6 and *Cxcl13*$^{-/-}$ mice were infected as described for Figure 1. Cells from wild type and *Cxcl13*$^{-/-}$ infected spleens were isolated at day 20 and the number of antigen-specific IFNγ-producing cells determined by ELISpot (C). Uninfected (B6 UI) and day 20-infected B6 and *Cxcl13*$^{-/-}$ mice received CFSE labeled ESAT-6 TCR Tg T cells and the frequency of Tg cells expressing CD69 12 hours after transfer was determined in the spleens by flow cytometry (D). The data points represent the mean (±SD) of values from four-five mice (A–F). * , $p \leq 0.05$. * * , $p \leq 0.005$. * * * , $p \leq 0.0005$, ns-not significant.